

# Manganese Abundances in the Globular Cluster $\omega$ Centauri

Katia Cunha & Verne V. Smith

*National Optical Astronomy Observatory, 950 N. Cherry Ave, Tucson, AZ, 85719 - USA*

Maria Bergemann

*Max-Planck Institute for Astrophysics, Karl-Schwarzschild Str. 1, 85741 Garching, Germany*

Nicholas B. Suntzeff

*Texas A&M University, Department of Physics and Astronomy & Mitchell Institute for Fundamental Physics and Astronomy, College Station, TX 77843-4242, USA*

David L. Lambert

*University of Texas, 1 University Station, C1400, Austin, TX 78712 USA*

## ABSTRACT

We present manganese abundances in 10 red-giant members of the globular cluster  $\omega$  Centauri; 8 stars are from the most metal-poor population (RGB MP and RGB MInt1) while two targets are members of the more metal rich groups (RGB MInt2 and MInt3). This is the first time Mn abundances have been studied in this peculiar stellar system. The LTE values of  $[\text{Mn}/\text{Fe}]$  in  $\omega$  Cen overlap those of Milky Way stars in the metal poor  $\omega$  Cen populations ( $[\text{Fe}/\text{H}] \sim -1.5$  to  $-1.8$ ), however unlike what is observed in Milky Way halo and disk stars,  $[\text{Mn}/\text{Fe}]$  declines in the two more metal-rich RGB MInt2 and MInt3 targets. Non-LTE calculations were carried out in order to derive corrections to the LTE Mn abundances. The non-LTE results for  $\omega$  Cen in comparison with the non-LTE  $[\text{Mn}/\text{Fe}]$  versus  $[\text{Fe}/\text{H}]$  trend obtained for the Milky Way confirm and strengthen the conclusion that the manganese behavior in  $\omega$  Cen is distinct. These results suggest that low-metallicity supernovae (with metallicities  $\leq -2$ ) of either Type II or Type Ia dominated the enrichment of the more metal-rich stars in  $\omega$  Cen. The dominance of low-metallicity stars in the chemical evolution of  $\omega$  Cen has been noted previously in the s-process elements where enrichment from metal-poor AGB stars is indicated. In addition, copper, which also has metallicity dependent yields, exhibits lower values of  $[\text{Cu}/\text{Fe}]$  in the RGB MInt2 and MInt3  $\omega$  Cen populations.

*Subject headings:* globular clusters: individual ( $\omega$  Centauri)

## 1. Introduction

The abundance ratios of chemical elements which have different nucleosynthetic origins can be used to constrain the history of chemical evolution in different types of stellar populations. This is because stellar sources, such as massive stars that undergo core-collapse and explode as supernovae of Types II or Ib/Ic, or binary systems that become Type Ia supernovae (SNe Ia), or asymptotic giant branch (AGB) stars, produce and return to the interstellar medium different element abundance ratios on differing timescales. Abundance ratios of certain elements can thus be used to explore which stars and in which proportions have contributed to chemical evolution within stellar populations in galaxies.

Of particular interest to chemical evolution of a stellar system are those elements whose yields may depend on the metallicity of the progenitor star. Metallicity-dependent abundance patterns can retain ‘memory’ of the metallicity distributions of their stellar populations, regardless of how the overall metallicity of the parent galaxy evolves. One important element whose production may be metallicity dependent is manganese ( $Z=25$ ), which falls within the iron peak. Manganese is produced in both core collapse supernovae (CC SNe) and SNe Ia, but the relative amounts from these two sources are not well constrained. Manganese has one stable isotope,  $^{55}\text{Mn}$ ; this element is synthesized as a result of explosive incomplete silicon burning (see, e.g., Thielemann et al. 2007 for a more complete discussion).

Woosley & Weaver (1995), for example, model nucleosynthesis of massive stars exploding as supernovae of Type II (SNe II) and find increasing Mn yields with increasing metallicity. Convolution of the Mn yields from the Woosley & Weaver (1995) models with a Salpeter mass function leads to values of  $[\text{Mn}/\text{Fe}]$  that decline steadily to  $-0.3$  at  $[\text{Fe}/\text{H}]=-1$  and then to  $-0.5$  at  $[\text{Fe}/\text{H}]=-2$ . A decrease of  $[\text{Mn}/\text{Fe}]$  ratios with metallicity is reported in the LTE Mn I abundance analyses of Galactic stars such as Gratton (1989), Reddy et al. (2003; 2006), Johnson (2002), Cayrel et al. (2004), or Fetzing et al. (2007). Recent results from Bergemann & Gehren (2008), however, indicate that the LTE approximation underestimates the abundances based on Mn I lines by 0.1 - 0.4 dex, with non-LTE effects being most pronounced in stellar atmospheres with low metal content. In the metallicity range investigated by Bergemann & Gehren (2008),  $-2.5 < [\text{Fe}/\text{H}] < 0$ , the non-LTE  $[\text{Mn}/\text{Fe}]$  ratios in late-type stars are approximately solar. The flat  $[\text{Mn}/\text{Fe}]$  trend with  $[\text{Fe}/\text{H}]$  is in general agreement with the SNe II yields of Chieffi & Limongi (2004) who do not predict a strong depletion of Mn relative to Fe at low metallicities.

Manganese yields from SNe Ia models can span a range of values depending on the explosion mechanism, such as slow or fast deflagrations, or deflagration-detonation events. Iwamoto et al. (1999) investigate a variety of models and find no large differences in Mn/Fe yields (i.e., less than a factor of  $\sim 2$ ) from models driven by both slow and fast deflagrations, as

well as deflagration-detonations, having different initial metallicities. Badenes et al. (2008) computed nucleosynthesis from 4 delayed detonation models, with different metallicities, as well as one deflagration model. This group finds that Mn yields decline with decreasing metallicity, despite the differences in the explosion mechanisms and initial conditions of the models.

In addition to the results for the Galactic thin disk, thick disk and halo noted above, McWilliam et al. (2003) added two other populations to the studies of manganese by measuring LTE  $[\text{Mn}/\text{Fe}]$  abundances for stellar members of the Sagittarius dwarf spheroidal galaxy and stars from the Galactic bulge. Both systems exhibited somewhat different behaviors of  $[\text{Mn}/\text{Fe}]$  with  $[\text{Fe}/\text{H}]$ , with the Sgr dwarf galaxy stars having values of  $[\text{Mn}/\text{Fe}]$  that fall below the general LTE trend found for Milky Way disk or halo stars at a given  $[\text{Fe}/\text{H}]$ . Bulge stars exhibit opposite behavior, with their values of  $[\text{Mn}/\text{Fe}]$  falling above the trend defined by the Milky Way disk and halo stars.

The goal of this study is to add another distinct stellar population to analyses of manganese and its chemical evolution in different Galactic environments.  $\omega$  Cen exhibits some peculiar characteristics in the nature of its chemical evolution, with perhaps the most striking being the large increase in the abundances of the heavy s-process elements (such as Ba or La) as the overall metallicity of cluster stars, measured by such elements as Fe, Ca, or Ti, increases (e.g. Norris & Da Costa 1995).  $\omega$  Centauri, although historically classified as a globular cluster, is now thought possibly to be a surviving remnant of a captured small galaxy, with multiple populations spanning a large range in metallicity (for a more detailed discussion see the review by Smith 2004). Recently, Carretta et al. (2010) have pointed out similarities between the  $\omega$  Cen populations and those from the Sagittarius dwarf galaxy. Five distinct stellar populations each with a different metallicity have been identified by Pancino et al. (2000) and Sollima et al. (2005). These studies label the distinct red giant branches from the  $\omega$  Cen populations as RGB MP (metal-poor); RGB MInt1; RGB MInt2; RGB MInt3 (intermediate metallicities); and RGB-a (anomalous, with the highest metallicity).

Manganese abundances are presented here for the first time in  $\omega$  Cen stars, with the sample consisting of 10 targets; 8 red giants are from the most metal poor populations (RGB MP and RGB MInt1) and 2 stars are from the more metal rich RGB MInt2 and MInt3. These  $\omega$  Cen stars have been analyzed in previous studies (Smith et al. 2000; Cunha et al. 2002), however Mn was not included in the analysis.

## 2. Observations and Stellar Parameters

The high-resolution spectra analyzed in this study were obtained using the cassegrain echelle spectrograph on the CTIO 4m Blanco telescope. This data set is the same as analyzed in the previous abundance study by Smith et al. (2000). The stellar parameters and microturbulent velocities adopted for the target stars are also from this previous study (see Smith et al. 2000 for details). In brief summary, effective temperatures and microturbulence parameters were found from the condition that the abundances derived from the LTE analysis of Fe I lines of different excitation potentials and equivalent widths were equal. In addition,  $T_{\text{eff}}$ s were estimated from the photometric indices (B-V) and (V-K). Surface gravities, and thus metallicities, were determined from the condition of ionization equilibrium of Fe, i.e. that Fe I and Fe II lines computed under LTE yield equal abundances. The adopted values of  $T_{\text{eff}}$ , surface gravity (as  $\log g$ ), Fe abundances ( $A(\text{Fe})$ ), and microturbulent velocities ( $\xi$ ) for the  $\omega$  Cen targets are listed in Table 1. The typical uncertainties are  $\pm 100\text{K}$  in  $T_{\text{eff}}$ ,  $\pm 0.3$  dex in  $\log g$ ,  $\pm 0.12$  dex in  $A(\text{Fe})$ , and  $\pm 0.3 \text{ km s}^{-1}$  in  $\xi$ .

In addition to  $\omega$  Cen stars, 4 M4 red giants were included in this study. M4 is a well-studied Galactic globular cluster and provides a comparison object for  $\omega$  Cen. The M4 targets were observed with the same echelle spectrograph on the CTIO 4m and these spectra were previously analyzed by Drake et al. (1992), although Mn was not one of the elements analyzed in that study. Table 1 includes the stellar parameters ( $T_{\text{eff}}$ ,  $\log g$ ,  $\xi$ ) and iron abundances for M4 stars taken from Drake et al. (1992).

## 3. Manganese Abundance Analysis

Manganese abundances were derived from LTE spectrum synthesis using the code MOOG (Snedden 1973). The model atmospheres adopted in this analysis are the same as in Cunha et al. (2002) and are taken from the Bell et al. (1976) MARCS grid for metal-poor giants. The use of Bell et al. (1976) models is justified as comparisons to the current MARCS grid of model atmospheres (Gustafsson et al. 2008) indicate no measurable differences in the Mn I abundances for the range in effective temperatures and surface gravities of the studied stars.

The abundance of manganese in the target red giants were derived from Mn I lines near  $\lambda$  6000Å. Three Mn I lines are available in this spectral region:  $\lambda\lambda$  6013.50Å; 6016.64Å; and 6021.80Å. In this study, only two Mn I transitions were analyzed as the Mn I line at 6016.64Å is blended with a Fe I transition at 6016.604Å. Our linelist in the 6015Å region included this Fe I line with a  $g\text{-value}$  from the Kurucz database ( $\log gf = -1.82$ ; from May et

al. 1974 but renormalized to an average multiplet). However, the solar spectrum could not be adequately fit with the Kurucz gf-value as the synthetic Mn I line at 6016Å was clearly too broad when compared to the observed solar spectrum. Test calculations indicated that the Fe I line gf-value would have to be decreased significantly in order to properly match the width of the Mn I line in the solar spectrum. Given the uncertainties in the gf-value of the blending Fe I line, the Mn I line at 6016.64Å was rejected from this study.

The inclusion of hyperfine splitting (hfs) in the computation of synthetic spectra is a requirement in order to properly analyze the Mn I transitions, which are affected by significant hyperfine splitting. The hfs data for both Mn I lines in this study were taken from Table 1 in Prochaska & McWilliam (2000). We have recomputed the hyperfine structure of the 6013Å Mn I line using the magnetic dipole and electric quadrupole interaction constants for the upper level (e6S) of multiplet 16 from Brodzinski (1987) and for the lower level (z6P\*) from Handrich et al. (1969). The line equivalent widths of the 6013Å lines computed with our hfs and that of Prochaska & McWilliam (2000) agree to within 1%. The gf-values of Mn I  $\lambda$  6013.50Å and 6021.80Å are from Blackwell-Whitehead & Bergemann (2007) and these are the same adopted in Bergemann & Gehren (2007). Table 2 provides the line list used in the abundance analysis of manganese. Additional atomic lines from the Kurucz line list were added along with CN lines from Davis & Phillips (1963; which were kindly provided to us in digital form by A. McWilliam).

Synthetic spectra were computed and manganese abundances were adjusted in order to best match the observed Mn I profiles. The Unsöld approximation (Unsöld 1968) was adopted, without enhancements, for the van der Waals damping. The Unsöld interaction potentials are known to underestimate widths of strong metal lines in the solar spectrum (Gehren et al. 2001a,b), and another approach to compute the line broadening due to elastic collisions with H I atoms was developed by Anstee & O’Mara (1995). However, for the parameters of stars in our analysis the differences in the profiles of Mn I lines of multiplet 16 computed with the Unsöld or Anstee & O’Mara (1995) formalisms are very small. The spectral region containing the Mn I features is illustrated in Figure 1 which shows synthetic and observed spectra for the target star ROA383. As a comparison the Mn I lines were also synthesized in the well-studied giant Arcturus using the spectral atlas from Hinkle et al. (2000). The stellar parameters adopted for Arcturus were  $T_{\text{eff}} = 4300$  K,  $\log g = 1.7$ , and metallicity,  $[\text{m}/\text{H}] = -0.6$  (Smith et al. 2000). This analysis of Arcturus yielded a Mn abundance of  $A(\text{Mn}) = 4.70$ . The abundances of Arcturus are also included in Table 1.

Uncertainties in the primary stellar parameters,  $T_{\text{eff}}$ , surface gravity, and the microturbulent velocity all affect the derived abundance. In order to estimate the errors in the Mn I abundances introduced by uncertainties in stellar parameters, the following sensitivities

to each variable were calculated:  $(\Delta A_{\text{Mn}}/\Delta T_{\text{eff}})_{-100\text{K}} = -0.22$ ,  $(\Delta A_{\text{Mn}}/\Delta \xi)_{+0.3\text{km/s}} = -0.06$ , and  $(\Delta A_{\text{Mn}}/\Delta \log g)_{+0.3} = +0.02$ . A quadrature sum of these sensitivities results in estimated uncertainties in the manganese abundances from the Mn I lines to be about  $\pm 0.23$ , with temperature errors being, by far, the dominant term.

### 3.1. Non-LTE Effects

The manganese abundance analysis in this study (and almost all previous studies of manganese in the literature) has adopted the simplifying assumption of LTE for the Mn I lines. Recently, however, non-LTE calculations of the Mn I lines have been done for the Sun (Bergemann & Gehren 2007) and for a sample of metal-poor dwarfs and subgiants (Bergemann & Gehren 2008). Bergemann & Gehren (2008) find that within the range of effective temperatures from 5000 - 6200K, surface gravities from 3.4 to 4.6 in  $\log g$ , and metallicities from solar down to -3 in  $[\text{Fe}/\text{H}]$ , the non-LTE corrections decrease with decreasing  $T_{\text{eff}}$ , increase with decreasing metallicity, and increase slightly with decreasing gravity.

Test non-LTE calculations were done for a few stars in our sample in order to investigate the influence of non-LTE effects on line formation of the Mn I sample lines  $\lambda 6013\text{\AA}$  and  $6021\text{\AA}$ . Five targets were selected in order to cover the range in stellar parameters and metallicities of the studied sample. The statistical equilibrium calculations for Mn were performed with the DETAIL code (Butler & Giddings 1985) using a manganese model atom from Bergemann & Gehren (2007). The model atom has three ionization stages containing 459 levels and 2809 radiative transitions. Wavelengths and oscillator strengths are taken from Kurucz & Bell (1995). The cross-sections of inelastic collisions with H I atoms are computed with the Drawin's formula in the version of Steenbock & Holweger (1984) and multiplied by a scaling factor of 0.05. This value was found from the analysis of Mn I lines in the solar and stellar spectra (Bergemann & Gehren 2007; 2008). Photoionization cross-sections were computed from the Kramer's formula using effective principle quantum numbers. The Mn model is complete up to the Mn III ground state. This is important for cool low-gravity atmospheres, because the number densities of neutral and singly-ionized atoms at line formation depths are comparable and statistical equilibrium of Mn is established by non-LTE processes in the atoms of both ionization stages. The model atmospheres for Mn statistical equilibrium calculations in this work were computed by Grupp (2010; private communication) with the code MAFAGS-OS (Grupp 2004 a, b). These models are standard plane parallel static LTE models, and they are virtually identical to the respective model atmospheres used in the LTE analysis; in particular, the temperature stratifications agree

to within 50K at  $-2.5 < \log \tau < 1$  (see Figure 2). Since non-LTE effects also depend on the elemental abundance, the statistical equilibrium calculations were performed with Mn abundances derived from the LTE analysis.

The detailed discussion of non-LTE equilibria in Mn for solar-type stars was given in Bergemann & Gehren (2007; 2008). The character of interaction processes does not change for stellar parameters, which form the basis of the current analysis. The diagrams of level departure coefficients <sup>1</sup> for two model atmospheres from our sample are shown in Figure 3. Since in this study we are solely interested in investigating the formation of the Mn I lines of multiplet 16, only selected levels are indicated. The Mn I levels are underpopulated at optical depths  $\log \tau(500nm) < 0.7$ ,  $b_i < 1$ , which is due to line pumping (see Bergemann & Gehren 2007) combined with overionization from intermediate-excitation Mn I levels. Overionization from densely-populated low-excitation Mn I levels, which is the dominant non-LTE effect in solar-type stars at sub-solar metallicities, is not very efficient at the low temperatures encountered in the atmospheres of giants. Also, collisional interaction of the majority of levels is very weak due to low densities and metallicities of the models. This is manifested in a rather irregular behavior of departure coefficients of Mn I levels with depth, as seen in Figure 3.

The departure coefficients were used to compute non-LTE abundance corrections  $\Delta_{\text{non-LTE}}$  (defined as the difference in abundances required to fit non-LTE and LTE profiles,  $\Delta_{\text{non-LTE}} = A_{\text{non-LTE}} - A_{\text{LTE}}$ ) to the lines of multiplet 16 for five stars from our sample. The non-LTE corrections obtained for these stars are found in Table 3.  $\Delta_{\text{non-LTE}}$  are positive and range from +0.05 dex for the models with higher metallicities to +0.3 dex for the model atmosphere of ROA 213 with  $[\text{Fe}/\text{H}] = -2$ . The variations of  $\Delta_{\text{non-LTE}}$  between models can be understood from the inspection of departure coefficients, which define the behavior of line opacities  $\kappa_{\nu}^l \sim b_i$  and source functions  $S^l \approx \frac{b_j}{b_i} B_{\nu}^l$ , where  $B_{\nu}^l$  is the Planck function and indices  $j$  and  $i$  refer to the upper and lower level of a transition, respectively. At  $[\text{Fe}/\text{H}] \sim -1$ , both Mn I lines of multiplet 16 are strong enough and their non-LTE corrections are determined by the competition of  $S^l > B_{\nu}^l$  in the wings and  $S^l < B_{\nu}^l$  in the core. The latter condition implies a strengthening of a line, thus non-LTE corrections are small. At a decreased metallicity,  $[\text{Fe}/\text{H}] = -2$ , the lines become weak and are formed in the deeper layers, where  $S^l > B_{\nu}^l$ , and also  $b_i < 1$ . The raised non-LTE source function and decreased opacity cause significant weakening of the line, and, thus, large positive non-LTE abundance corrections.

---

<sup>1</sup>Departure coefficients characterize deviations of number densities of atoms in the level  $i$  from their LTE values,  $b_i = n_i^{\text{non-LTE}}/n_i^{\text{LTE}}$

Thus, for the range of stellar parameters investigated here, the magnitude of the non-LTE abundance corrections for both Mn I lines of multiplet 16 is determined primarily by metallicity.  $\Delta_{\text{non-LTE}}$  are largest ( $\sim 0.3$  dex) for the most metal-poor  $\omega$  Cen giant ( $[\text{Fe}/\text{H}] = -2$ ), while for the red giants with larger metallicity ( $[\text{Fe}/\text{H}] = -1$ ) and low Mn abundances,  $\Delta_{\text{non-LTE}} \sim 0.1$  dex

## 4. Discussion

The final LTE manganese abundances that are shown in Table 1 are combined with iron abundances (from Smith et al. 2000 for  $\omega$  Cen and Drake et al. 1992 for M4) and compared with abundances from other stellar samples. The discussion begins with a comparison of Mn abundances in  $\omega$  Cen with stars from the thin disk, thick disk, and halo, as well as Sgr dwarf galaxy members. This is then followed by a section that compares  $\omega$  Cen with those abundances from a large sample of Milky Way globular cluster giants and field stars. The discussion concludes by highlighting how the manganese abundances provide additional insight into chemical evolution within  $\omega$  Cen.

### 4.1. $[\text{Mn}/\text{Fe}]$ in $\omega$ Cen, Milky Way Field Stars and the Sagittarius Dwarf Galaxy

The initial comparison of  $\omega$  Cen stars with other stellar populations is shown in Figure 4, where the LTE abundance ratios of Ca/Fe and Mn/Fe, computed as  $A(\text{Ca or Mn}) - A(\text{Fe})$ , are shown versus  $A(\text{Fe})$ , with Ca/Fe plotted in the top panel and Mn/Fe in the bottom panel. It is of interest to discuss calcium results first, as Ca is a well-studied  $\alpha$ -element whose yields are not expected to be metallicity dependant. The solar values are indicated by the solar symbols and abundances plotted this way can easily be transformed to values of  $[\text{Ca}/\text{Fe}]$  and  $[\text{Mn}/\text{Fe}]$  by using the absolute solar values ( $A(\text{Ca})_{\odot}=6.34$ ,  $A(\text{Mn})_{\odot}=5.43$ , and  $A(\text{Fe})_{\odot}=7.45$ ; Asplund et al. 2009). The Milky Way field-star samples are plotted as blue small symbols and are taken from Reddy et al. (2003; 2006; open circles); Fulbright (2002; open squares); Johnson (2002; open squares); Cayrel et al. (2004; open triangles) and McWilliam et al. (1995; open pentagons). We also added the results for metal-rich  $\omega$  Cen stars by Pancino et al. (2002; red filled squares) and the Sagittarius dwarf results by McWilliam et al. (2003) and Sbordone et al. (2007) are represented as green asterisks.

Focussing first on LTE Ca/Fe in the field stars, the overall trends are clear, with values of Ca/Fe increasing with decreasing Fe abundance, which befits calcium’s classification as

an  $\alpha$ -element (Figure 4; top panel). Note that in this figure, no distinction is made between thin and thick disk populations, which may account for some of the scatter in Ca/Fe at disk metallicities. In this panel, the  $\omega$  Cen members follow roughly the LTE trend defined by the Milky Way field stars (as do the Sgr dwarf galaxy stars, although the most metal-rich Sgr stars tend to fall below the Ca/Fe values defined by the Galactic field stars). Note that the histogram plotted within the top panel of Figure 4 represents the Fe-abundance distribution function derived for  $\omega$  Cen by Sollima et al. (2005) and is included as a schematic representation of where the  $\omega$  Cen stars studied here, along with those from Pancino et al. (2002) fall within the overall metallicity distribution of the cluster.

Turning now to the bottom panel, with Mn/Fe plotted versus A(Fe) (both quantities being LTE values), the trend for the Milky Way field stars can be described as one in which Mn/Fe declines steadily with decreasing Fe abundance, to values of  $\sim -0.4$  dex below solar at iron abundances about 1/10 solar. The ratio then remains fairly constant, albeit with considerable scatter, which may be due to systematic effects between different studies, as metallicity continues to decrease. There may be another downturn in Mn/Fe at the very lowest metallicities, however the non-LTE corrections found by Bergemann & Gehren (2008) predict increasingly large corrections as the metallicity declines, so part of this apparent decline at very low Fe abundance may be due to non-LTE effects, such that the value of Mn/Fe is more nearly constant. As noted by McWilliam et al. (2003), the Sgr stars included in Figure 4 (bottom panel) fall below the Mn/Fe versus Fe trend set by the Milky Way stars, with the offset being  $\sim 0.2$  dex.

With the inclusion of  $\omega$  Cen Mn/Fe ratios, the differences between the Milky Way populations become even more extreme than Sgr, with a decline in Mn/Fe as Fe increases in  $\omega$  Cen. In the most metal-rich  $\omega$  Cen stars in this sample the values of Mn/Fe fall about 0.6-0.7 dex below the LTE trend established for the field stars. This offset between  $\omega$  Cen and Milky Way stars is reminiscent of what was found for Cu/Fe by Cunha et al. (2002) for  $\omega$  Cen, and was also found for Cu/Fe in Sgr by McWilliam & Smecker-Hane (2005). The chemical evolution of manganese in  $\omega$  Cen is yet another observation that implicates  $\omega$  Cen as a chemically distinct population when compared to the Milky Way and that can be more closely associated with abundance patterns in small galaxies at comparable metallicities. We note, however, that in  $\omega$  Cen there are significantly more metal-rich stars (e.g. Norris & Da Costa 1995; Pancino et al. 2002) that reach near-solar metallicities. So far these stars have not yet been analyzed for Mn.

As discussed in Section 3.1, the non-LTE Mn results indicate it is unlikely that the low ratios of Mn/Fe observed in  $\omega$  Cen result from non-LTE effects. In fact, a direct application of the non-LTE corrections to the  $\omega$  Cen stars would increase the differences in Mn/Fe

between the metal-poor and metal-rich members of  $\omega$  Cen, as shown in the top panel of Figure 5.

One can also compare non-LTE Mn abundances in Milky Way field stars with the non-LTE results for the  $\omega$  Cen stars derived here. Bergemann & Gehren (2008) provide the Milky Way field-star sample by having analyzed 14 stars spanning a range in  $[\text{Fe}/\text{H}]$  from  $\sim 0.0$  to  $-2.5$ . In this case, a comparison of  $\omega$  Cen with the field stars leads to an even more striking difference, with Bergemann & Gehren (2008) finding essentially constant values of  $[\text{Mn}/\text{Fe}]$  not very different from solar across the observed range in  $[\text{Fe}/\text{H}]$ : the mean and standard deviation are  $[\text{Mn}/\text{Fe}] = -0.05 \pm 0.11$ , with no significant trend found with metallicity. The  $\omega$  Cen stars fall well below these values, with  $\text{Mn}/\text{Fe}$  decreasing slightly with increasing metallicity. Differences between  $\omega$  Cen stars and the Milky Way field stars exist whether the comparison is with LTE or non-LTE abundances.

There still remains concern that perhaps ratioing non-LTE Mn I abundances with LTE Fe I abundances might induce spurious values of  $\text{Mn}/\text{Fe}$  so as to perturb significantly the location of the  $\omega$  Cen giants in the  $\text{Mn}/\text{Fe} - A(\text{Fe})$  plane. Since non-LTE calculations of Fe I and Fe II in cool red giants remain questionable, the test of Mn I to Fe can be expanded to include abundances from Fe II (since in these red giants virtually all iron is in the form of Fe I + Fe II). Such a test is possible to carry out by using results from Smith et al. (2000), who included both Fe I and Fe II in their analysis.

Smith et al. (2000) forced equal abundances from both Fe I and Fe II as a way of setting the surface gravities, although another method to derive surface gravities is to use the rather well-defined luminosities of the  $\omega$  Cen red giants (which are in Smith et al. 2000 Table 1) in combination with  $T_{\text{eff}}$  and stellar mass,  $M$ . The luminosities in Smith et al. were derived by using a distance modulus  $(m-M)=13.6$  and an  $E(B-V)=0.11$  with K-magnitudes to determine  $M_K$ . Bolometric corrections were then taken from Bessel et al. (1998) to arrive at  $M_{\text{bol}}$ . Since  $L \propto R^2 T_{\text{eff}}^4$  and  $g \propto MxR^{-2}$ , then  $g \propto MxL^{-1}xT_{\text{eff}}^4$ . With known  $T_{\text{eff}}$  and  $L$ , these can be combined with the rather restricted range of masses allowed for old, low-mass red giants to derive "evolutionary" gravities; in this case, we use  $0.8M_{\odot}$  for the masses of the  $\omega$  Cen red giants. The evolutionary gravities can then be compared to the spectroscopic gravities to search for systematics or large scatter that would lead to large differences in the LTE Fe I and Fe II abundances. Such a comparison for the 10  $\omega$  Cen red giants finds no large differences, with the result that the mean and standard deviation of  $\Delta_{\log g}(\text{evolutionary } \log g - \text{spectroscopic } \log g) = +0.11 \pm 0.18$  dex. This small offset and scatter is within the uncertainties in the spectroscopic gravities themselves, as well as the masses. Employing the evolutionary gravities would lead to Fe II abundances that are only slightly larger, in the mean, by  $+0.12$  dex. Using various combinations of spectroscopic or evolutionary gravities

and either Fe I or Fe II abundances, will not alter the conclusion that the metal-rich  $\omega$  Cen stars exhibit low values of Mn/Fe when compared to other stellar populations. The low values of Mn/Fe in the more metal-rich  $\omega$  Cen stars, relative to Milky Way field stars, is a real effect that needs to be explained by chemical evolution within this peculiar stellar system.

#### 4.2. [Mn/Fe] in $\omega$ Cen and Milky Way Globular Clusters

It has been previously shown that the general pattern of globular cluster abundances (with very few exceptions) typically follows the trends observed for the disk and halo at a given iron abundance. Sobeck et al. (2006) derived Mn abundances in more than 200 giant stars in 19 Milky Way globular clusters, along with about 200 field giants. Their results for [Mn/Fe] versus [Fe/H] revealed no significant differences between the globular clusters and field populations.

A comparison of our derived LTE abundances for  $\omega$  Cen and M4 with the Sobeck et al. (2006) LTE results are of particular interest as globular cluster giants in their sample have similar stellar parameters ( $T_{\text{eff}}$  and  $\log g$ ) to the target stars studied here. It should be noted that both studies analyzed the same Mn I lines although Sobeck et al. adopted the gf-values from Booth et al. (1984), which are higher than the ones adopted here. Figure 5 (bottom panel) illustrates a comparison between the Mn/Fe versus A(Fe) abundance results in the two studies; the Sobeck et al. (2006) abundances in the figure were adjusted in order to account for differences in the adopted gf-values. Since the stellar parameters in Sobeck et al. (2006) are similar to those for the  $\omega$  Cen and M4 stars studied here, it is likely that non-LTE corrections to their results will be similar to those computed here. The trend of increasing positive non-LTE abundance corrections for the Mn I lines with decreasing metallicity would likely apply to the Sobeck et al. (2006) results. Whether comparing LTE abundances or likely non-LTE abundances, as with Figure 4 (bottom panel), this demonstrates that  $\omega$  Cen is different from the typical Milky Way globular cluster population in its low values of Mn/Fe.

To reinforce the differences found in values of Mn/Fe in the more metal-rich  $\omega$  Cen red giants, when compared to other globular cluster red giants, the results derived here for the 4 M4 targets are also plotted in the bottom panel of Figure 5 (as filled green squares). Recall that these M4 red giants were observed with the same spectrograph and their analysis was the same as that used for the  $\omega$  Cen sample. The location of the M4 abundances derived for Mn/Fe and A(Fe) falls within the scatter of results from the Sobeck et al. (2006) globular cluster abundances. In fact, two of the M4 stars analyzed here are in the Sobeck et al. (2006) study and the black lines from these two M4 stars connect the abundances derived in this

study to those values from Sobeck et al. (2006): the agreement between the two studies is very good. The two most metal-rich  $\omega$  Cen red giants remain depressed in their Mn/Fe abundance ratios when compared to stars of similar metallicity in M4.

### 4.3. Manganese and the Stellar Populations of $\omega$ Cen

Having established low Mn/Fe ratios in the two most metal-rich  $\omega$  Cen stars analyzed here, it is of interest to place these depressed Mn/Fe ratios in the context of the star formation history of  $\omega$  Cen and its chemical evolution. As mentioned in the introduction, large-field photometric surveys, such as those of Lee et al. (1999), Pacino et al. (2000), or Sollima et al. (2005), which include tens of thousands, or up to 100,000 stars, have identified discrete red giant branches (RGBs) in color-magnitude diagrams (CMDs) in, for example, B versus B-V or I versus B-I. Such discrete RGBs represent stellar populations, each having a reasonably well-defined metallicity and probably age.

Sollima et al.(2005) identified 5 distinct RGBs, which can be ordered by metallicity. These RGBs have been labelled as MP (for metal poor), then 3 intermediate-metallicity branches ordered in increasing metallicity as MInt1, MInt2, and MInt3, and finally a quite metal-rich group called RGB-a ('a' for anomalous). These separate RGBs are clearly visible in the Sollima et al. (2005) MDF plotted schematically in the top panel of Figure 4.

Sollima et al. (2005) define metallicity limits for each of the RGBs and their definition can be used to associate each of the  $\omega$  Cen red giants here with one of the branches. The last column of Table 1 lists this population classification. Of course there is uncertainty in this classification due to both uncertainties in the Fe abundances from Smith et al. (2000) and to overlap in neighboring RGBs. Uncertainties in  $A(\text{Fe})$  are  $\sim\pm 0.1$  dex and the RGB separations are about 0.2 dex, so the classification uncertainties are expected to be confined to a neighboring RGB. Within this classification scheme, the two stars having significantly low Mn/Fe ratios (ROA219 and ROA324) are members of MInt2 and MInt3. The MInt2 and MInt3 populations are part of the extended metal-rich tail, with most (if not all) of the Fe arising from CC SNe enrichment. In addition, these stars exhibit large s-process enhancements, which indicates substantial enrichment from low-metallicity AGB stars (Smith et al. 2000). Pacino et al. (2002) analyzed iron, copper and  $\alpha$ -elements and found no measurable SN Ia enrichment in 3 stars from the MInt3 and MInt2 populations, but did find such enrichment in 3 RGB-a stars (their Ca/Fe ratios are plotted in the top panel of Figure 4).

#### 4.3.1. *The effect of He enhancements on the Mn Abundances*

In addition to the peculiar heavy-element chemical evolution in  $\omega$  Cen, the presence of a blue main-sequence (Bedin et al. 2004) that is more metal-rich than the red main-sequence (Piotto et al. 2005) indicates significant He-enrichment may accompany the overall metallicity increase. It has been estimated by Norris (2004) that a He overabundance of  $\Delta Y \sim +0.15$  is required to explain the blue main-sequence stars. If this helium enhancement is correct, it suggests that some stars in this sample may have undergone some degree of He enrichment, so it is worth investigating if this might affect significantly Mn/Fe ratios.

Bohm-Vitense (1979) discussed the effects that enhanced He abundances would have on the strengths of spectral lines in late-type stellar atmospheres and her discussion can be used to estimate how an increased value of  $Y$  might affect, for example Mn/Fe ratios. Using her 'case b' (where electrons for  $H^-$  arise from metals which are partially ionized or mostly neutral, as expected in low temperature red giants) for neutral atomic lines in an atmosphere where the dominant continuous opacity is  $H^-$ , the dependence on helium abundance is small (line strength  $\propto (1 + 4y)^{1/6}(1 + y)^{2/3}$ , where  $y = N(\text{He})/N(\text{H})$ ). If the extremes in the  $\omega$  Cen populations are  $Y \sim 0.25$  and  $0.40$  (Sollima et al. 2008, in particular their Figure 2), the estimated effects on neutral metal lines from Bohm-Vitense's (1979) analysis would be small,  $y$  changing from  $0.08$  to  $0.17$  in her derived equation. In addition, the peculiarity of the  $\omega$  Cen stars is in the ratio of Mn/Fe, which is dependent on Mn I and Fe I lines, so effects due to enhanced He abundances would cancel to some degree. Bohm-Vitense (1979) also point out that, for this case of a cool atmosphere, He effects would be largest for lower ionization species and she notes that Ca I lines would be affected more than, say Fe I. Reinspection of the top panel of Figure 4 reveals that Ca/Fe in  $\omega$  Cen follows the trends defined by other stellar populations, suggesting that any He enhancements are probably not affecting significantly the derived metal abundances.

Finally, we have tested the effect of He-enhancement on the derived abundances by computing the Mn I line formation for the model atmosphere of the giant M4 2617 with  $\Delta Y = +0.1$ . The temperature stratification of this model is shown in Figure 2. We find that the profiles of the  $6013\text{\AA}$  and  $6021\text{\AA}$  Mn I lines computed with  $\Delta Y = +0.1$  model are almost identical to those computed with the model atmosphere with normal He abundance.

#### 4.4. Chemical Evolution within $\omega$ Cen as Revealed by Low Manganese Abundances

Recently, Cescutti et al. (2008) modelled the chemical evolution of manganese in three distinct stellar populations: Milky Way field stars (the Solar neighborhood, containing thin and thick disk members, as well as halo stars), the Bulge, and Sgr dwarf galaxy members. These three populations exhibit different behaviors, which can be summarized briefly as, at a given Fe abundance, Mn/Fe ratios in the Bulge fall above the Solar neighborhood stars, while Mn/Fe ratios in Sgr fall below the Solar neighborhood values. Note that all of these abundance studies used by Cescutti et al. (2008) are based on LTE analyses. Their results must be interpreted with caution, as non-LTE calculations need to be carried out in order to confirm or not the model conclusions.

Cescutti et al. (2008) use a model for the Solar neighborhood from François et al. (2004) and Chiappini et al. (1997), which assumes two Galactic accretion events, the first of which formed the halo and thick disk, while the second formed the thin disk. The infalling gas in the accretion events is taken to be primordial. For the Bulge, Cescutti et al. use a model with a rapid formation time (0.3-0.5 Gyr) and very efficient star formation (with the star formation per unit mass of gas being some 20 times larger than for the Solar vicinity). This rapid formation and vigorous star formation in the Bulge explains the large values of  $[\alpha/\text{Fe}]$  found in bulge stars by a number of studies (Cunha & Smith 2006; Zoccali et al. 2006; Lecureur et al. 2007; Fulbright et al. 2007; Meléndez et al. 2008, Ryde et al. 2010). In Sgr, it is assumed that stars formed over several Gyrs, with strong galactic winds driven by supernovae leading to significant gas loss. This galactic wind results in an overall decrease in star formation efficiency and explains the low values of  $[\alpha/\text{Fe}]$  observed in the more metal-rich Sgr members. When the above chemical evolution models are applied to tracking the chemical evolution of manganese, Cescutti et al. (2008) find that the best fits to the three trends of Mn/Fe versus  $A(\text{Fe})$  defined by each distinct population result when Mn is produced via metallicity-dependent yields in SN Ia.

If the Cescutti et al. (2008) model is applied to  $\omega$  Cen, the implication is that metal-enrichment at the metal-rich end of the distribution in this stellar system was driven by metal-poor SN Ia. This is a possibly viable model, as the majority of stars in  $\omega$  Cen are from the most metal-poor group (as evidenced by the histogram in the top panel of Figure 4), thus the time-delay of SN Ia to the chemical evolution would result in the metal-poor SN Ia systems contributing to the chemical makeup of the more metal-rich stars. Such SN Ia systems would be efficient producers of Fe, but would not synthesize much Mn, leading to low values of Mn/Fe. Quantitative predictions of Mn/Fe ratios await a detailed star formation history, probably with significant galactic winds, coupled to a chemical evolution model.

Such a model for  $\omega$  Cen has already been developed by Romano et al. (2007) and then applied by Romano & Matteucci (2007) to explain the low values of Cu/Fe found by Cunha et al. (2002) and Pancino et al. (2002). This model assumes that  $\omega$  Cen began its history as a dwarf spheroidal galaxy that evolved initially in isolation and whose chemical evolution was affected strongly by galactic winds (as with Sgr). The conclusion by Romano & Matteucci (2007) concerning copper, was that it was produced via a metallicity-dependent process in massive stars; in this case it is the weak s-process occurring during He-burning in these stars, with the neutron source being  $^{22}\text{Ne}(\alpha, n)^{25}\text{Mg}$ . Since the amount of  $^{22}\text{Ne}$  depends on the abundance of  $^{14}\text{N}$ , whose value depends on stellar metallicity, this renders the strength of the s-process proportional to metallicity.

Our result for  $\omega$  Cen is that Mn behaves as a metallicity-dependent element, in a similar manner to that of Cu, and may provide further constraints on both chemical evolution within this peculiar system, as well as the origins of both Mn and Cu. Note that Wylie de Boer et al. (2010) used low values of Cu/Fe as one indicator that stars in Kapteyn’s group may represent an  $\omega$  Cen stream. Our results here suggest that Mn/Fe would also be a useful tracer of possible  $\omega$  Cen tidal streams.

## 5. Conclusions

Manganese abundances have been measured for the first time in the peculiar globular cluster  $\omega$  Cen, with the analysis of 10 red giants spanning a range in metallicity from  $[\text{Fe}/\text{H}] = -1.9$  to  $-0.9$ . The analysis is based on Mn I lines using both LTE and non-LTE calculations to derive abundances. In addition, the possible effects of enhanced He abundances on derived Mn abundances were investigated for the more metal-rich  $\omega$  Cen giants and were found to be negligible.

The novel result is that two members from the more metal-rich populations with  $\omega$  Cen (RGB MInt2 and MInt3) exhibit low ratios of Mn/Fe in comparison to Galactic field stars, as well as other globular cluster stars at the same metallicity ( $[\text{Fe}/\text{H}] \sim -1$ ). Differences between  $\omega$  Cen and the other Milky Way populations exist whether the comparison is made using LTE or non-LTE abundances. The low abundances of Mn may indicate that low-metallicity progenitors to supernovae (of either core collapse or SNe Ia) dominated the production of manganese within  $\omega$  Cen. This result for Mn is similar to what has been noted previously for the behavior of copper (which in some nucleosynthesis processes has metallicity-dependent yields) in  $\omega$  Cen (Cunha et al. 2002).

The behavior of Mn in the more extreme metal-rich  $\omega$  Cen population (RGB-a) remains

to be probed. In future studies it would be of interest to determine Mn abundances in the most metal-rich  $\omega$  Cen population; for example, by analyzing Mn in the 3 most metal-rich red giants studied to date (ROA 300, WFI22068, and WFI222679) by Pancino et al. (2002). The behavior of the manganese abundances in these more metal-rich stars will provide further insight into both the origins of Mn and the nature of star formation within  $\omega$  Cen during the final throes of its chemical evolution.

MB thanks Dr. Frank Grupp for providing MAFAGS-OS model atmospheres for selected stars. This research was supported in part by the National Science Foundation (AST 06-46790 to KC and VVS). DLL thanks the Robert A. Welch Foundation for support via grant F-634.

## REFERENCES

- Anstee, S. D. & O'Mara, B. J. 1995, MNRAS, 276, 859
- Asplund, Martin; Grevesse, N., Sauval, A. J., & Scott, P. 2009, ARA&A 47, 481
- Badenes, C.; Bravo, E., Borkowski, K. J., & Domnguez, I. 2003, ApJ, 593, 358
- Badenes, C., Borkowski, K. J., & Bravo, E. 2005, ApJ, 624, 198
- Badenes, C., Bravo, E., & Hughes, J. P. 2008, ApJ, 680, L33
- Bedin, L. R., Piotto, G., Anderson, J., Cassisi, S., King, I. R., Momany, Y., Carraro, G. 2004, ApJ, 605, L125
- Bell, R. A., Eriksson, K., Gustafsson, B. E., & Nordlund, A. 1976, A&AS, 23, 37
- Bergemann, M. & Gehren, T. 2007, A&A, 473, 291
- Bergemann, M. & Gehren, T. 2008, A&A, 492, 823
- Bessell, M. S., Castelli, F., & Plez, B. 1998, A&A, 337, 321
- Blackwell-Whitehead, R. & Bergemann, M. 2007, A&A, 472, 43
- Bohm-Vitense, E. 1979, ApJ, 234, 521
- Booth, A. J., Blackwell, D. E., & Shallis, M. J. 1984, MNRAS, 209, 77
- Brodzinski, T., Kronfeldt, H. D., Kropp, J.-R. & Winkler, R. 1987, ZPhyD, 7, 161

- Butler, K. & Giddings, J. 1985, Newsletter on Analysis of Astronomical Spectra, University of London, vol. 9
- Carretta, E., Bragaglia, A., Gratton, R. G., Lucatello, S., Bellazzini, M., Catanzaro, G., Leone, F., Momany, Y., Piotto, G., & D’Orazi, V. 2010 arXiv1002.1963
- Cayrel, R., Depagne, E., Spite, M., Hill, V., Spite, F., François, P., Plez, B., Beers, T., Primas, F., Andersen, J., et al. 2004, *A&A*, 416, 1117
- Cescutti, G., Matteucci, F., Lanfranchi, G. A., & McWilliam, A. 2008, *A&A*, 491, 401
- Chiappini, C., Matteucci, F., & Gratton, R. 1997, *ApJ*, 477, 765
- Cunha, K., Smith, V. V., Suntzeff, N. B., Norris, J. E., Da Costa, G. S., & Plez, B. 2002, *AJ*, 124, 379
- Cunha, K., & Smith, V. V. 2006, *ApJ*, 651, 491
- Davis, S. P. & Philips, J. G. 1963, *The Red System of CN molecule* (Berkeley: University of California Press)
- Drake, J. J., Smith, V. V., & Suntzeff, N. B. 1992, *ApJ*, 395, L95
- Feltzing, S., Fohlman, M., & Bensby, T. 2007, *A&A*, 467, 665
- François, P., Matteucci, F., Cayrel, R., et al. 2004, *A&A*, 421, 613
- Fulbright, J. P., McWilliam, A., & Rich, R. M. 2007, *ApJ*, 661, 1152
- Fulbright, J. P. 2002, *AJ*, 123, 404
- Gehren, T., Butler, K., Mashonkina, L., Reetz, J. & Shi, J. 2001, *A&A*, 366, 981
- Gehren, T., Korn, A. J., & Shi, J. 2001, *A&A*, 380, 645
- Gratton R. 1989, *A&A*, 208, 171
- Grupp, F. 2004a, *A&A*, 420, 289
- Grupp, F. 2004b, *A&A*...426..309
- Gustafsson, B.; Edvardsson, B.; Eriksson, K.; Jørgensen, U. G.; Nordlund, A., & Plez, B. 2008, *A&A*, 486, 951
- Iwamoto, K., Brachwitz, F., Nomoto, K., Kishimoto, N., Umeda, H., Hix, W. R., Thielemann, F. 1999, *ApJS*, 125, 439

- Johnson, J. A. 2002, *ApJS*, 139, 219
- Handrich, E., Steudel, A., & Walther, H. 1969, *PhLA*, 29, 486
- Hinkle, K., Wallace, L., Valenti, J., & Harmer, D. 2000 *Visible and Near Infrared Atlas of the Arcturus Spectrum 3727-9300 A* (San Francisco: ASP)
- Kurucz, R. & Bell, B. CD-ROM No. 23. Cambridge, Mass.: Smithsonian Astrophysical Observatory, 1995.
- Lecureur, A., Hill, V., Zoccali, M., et al. 2007, *A&A*, 465, 799
- Lee, Y.-W., Joo, J. M., Sohn, Y.-J., Rey, S.-C., Lee, H.-C., Walker, A. R. 1999, *Nature*, 402, 55
- Chieffi, A. & Limongi, M. 2004, *ApJ*, 608, 405
- McWilliam, A., Preston, G. W., Sneden, C., & Searle, L. 1995, *AJ*, 109, 2757
- McWilliam, A. & Smecker-Hane, T. A. 2005, *ApJ*, 622, L29
- McWilliam, A. Rich, R. M. & Smecker-Hane, T. A. 2003, *ApJ*, 592, L21
- Meléndez, J., Asplund, M., Alves-Brito, A., et al. 2008, *A&A*, 484, L21
- Norris, J. & Da Costa, G. 1995, *ApJ*, 447, 680
- Norris, J. 2004, *ApJ*, 612, 25
- Pancino, E., Pasquini, L., Hill, V., Ferraro, F. R., & Bellazzini, M. 2002, *ApJ*, 568, L101
- Pancino, E. Ferraro, F. R., Bellazzini, M., Piotto, G., & Zoccali, M. 2000, *ApJ*, 534, 83
- Piotto, G., Villanova, S., Bedin, L. R. et al. 2005, *ApJ*, 621, 777
- Prochaska, J. X. & McWilliam, A. 2000, *ApJ*, 537, L57
- Reddy, B. E., Tomkin, J., Lambert, D. L., & Allende Prieto, C. 2003, *MNRAS*, 340, 304
- Reddy, B. E., Lambert, D. L., & Allende Prieto, C. 2006, *MNRAS*, 367, 1329
- Romano, D., Matteucci, F., Tosi, M., Pancino, E., Bellazzini, M., Ferraro, F. R., Limongi, M., Sollima, A. 2007, *MNRAS*, 376, 405
- Romano, D., & Matteucci, F. 2007, *MNRAS*, 378, 59

- Ryde, N., Gustafsson, B., Edvardsson, B. et al. 2010, *A&A*, 509, 20
- Sbordone, L., Bonifacio, P., Buonanno, R., Marconi, G., Monaco, L., & Zaggia, S. 2007, *A&A*, 235, 330
- Snedden, C. 1973, Ph.D. Thesis, The University of Texas at Austin
- Sobeck, J. S., Ivans, I. I., Simmerer, J. A., Sneden, C., Hoefflich, P., Fulbright, J. P., Kraft, R. P. 2006, *AJ*, 131, 2949
- Sollima, A., Pancino, E., Ferraro, F. R., Bellazzini, M., Straniero, O., & Pasquini, L. 2005, *MNRAS*, 357, 265
- Sollima, A., Ferraro, F. R., Pancino, E., & Bellazzini, M. 2008, *MmSAI*, 79, 342
- Smith, V. V., Suntzeff, N. B., Cunha, K., Gallino, R., Busso, M., Lambert, D. L., & Straniero, O. 2000, *AJ*, 119, 1239
- Smith, V. V. 2004, Smith, in *Origin and Evolution of the Elements*, ed. A. McWilliam & M. Rauch (Cambridge: Cambridge Univ. Press), 186
- Steenbock, W. & Holweger, H. 1984, *A&A*, 130, 319
- Thielemann, F.-K., Frhlich, C., Hirschi, R. et al. 2007, *Progress Particle Nuclear Phys.*, 59, 742007
- Unsöld, A. 1968, *Physik der Sternatmosphaeren, mit besonderer Beruecksichtigung der Sonne*, Heidelberg Taschenbuecher, Springer, Berlin
- Zoccali, M., Lecureur, A., Barbuy, B., et al. 2006, *A&A*, 457, L1
- Woosley, S. E. & Weaver, T. A. 1995, *ApJS*, 101, 1811
- Wylie-de Boer, E., Freeman, K. & Williams, 2010, *M. AJ*, 139, 636

Table 1. Program Stars and LTE Abundances

Star	$T_{\text{eff}}(\text{K})$	Log $g$	$\xi$ ( $\text{km}\cdot\text{s}^{-1}$ )	A(Fe)	A(Mn)	RGB Type
ROA102	4400	1.0	3.0	5.69	3.23	MP
ROA209	4500	1.2	2.0	5.72	3.36	MP
ROA213	4500	1.0	1.9	5.53	2.98	MP
ROA219	3900	0.7	1.7	6.25	3.34	Mint2
ROA236	4200	0.7	1.7	6.06	3.79	MInt1
ROA238	4550	1.2	1.7	5.72	3.14	MP
ROA245	4300	0.7	1.8	6.10	3.42	MInt1
ROA253	4300	0.7	1.9	6.08	3.50	MInt1
ROA324	4000	0.7	1.9	6.57	3.64	MInt3
ROA383	4400	1.0	1.8	5.89	3.35	MInt1
M4 2519	4480	1.3	1.8	6.27	3.85	...
M4 2617	4280	1.2	1.5	6.32	3.95	...
M4 3624	4300	1.3	1.5	6.28	3.99	...
M4 3612	4350	1.3	1.5	6.39	4.08	...
$\alpha$ Boo	4300	1.7	1.6	6.78	4.70	...

Table 2. Linelist for the Mn I line regions

$\lambda$ (Å)	Species	$\chi$ (eV)	Log gf
6013.020	Mo I	3.40	-0.955
6013.166	C I	8.65	-1.370
6013.168	$^{12}\text{C}^{14}\text{N}$	0.77	-2.798
6013.187	$^{12}\text{C}^{14}\text{N}$	1.87	-1.760
6013.206	Cr II	8.42	-3.522
6013.213	C I	8.65	-1.470
6013.218	$^{12}\text{C}^{14}\text{N}$	0.81	-2.305
6013.272	$^{12}\text{C}^{14}\text{N}$	1.76	-1.533
6013.293	V I	4.13	-4.513
6013.347	Fe II	8.07	-3.485
6013.383	Cr I	5.61	-3.938
6013.417	Ti I	1.07	-3.100
6013.420	Ce I	0.30	-0.526
6013.478	Mn I	3.07	-0.946
6013.499	Mn I	3.07	-1.158
6013.518	Mn I	3.07	-1.431
6013.527	Mn I	3.07	-1.635
6013.533	Mn I	3.07	-1.841
6013.538	Mn I	3.07	-1.489
6013.547	Mn I	3.07	-1.510
6013.550	$^{12}\text{C}^{14}\text{N}$	0.82	-2.014
6013.552	Mn I	3.07	-1.665
6013.556	$^{12}\text{C}^{14}\text{N}$	0.76	-2.596
6013.562	Mn I	3.07	-1.987
6013.566	Mn I	3.07	-2.033
6013.567	Mn I	3.07	-2.589
6013.568	Mn I	3.07	-2.209
6013.640	Co I	4.48	-2.870
6013.734	V II	6.52	-4.633
6013.773	$^{12}\text{C}^{14}\text{N}$	1.70	-1.922
6013.962	Ti II	8.11	-2.575

Table 2—Continued

$\lambda$ (Å)	Species	$\chi$ (eV)	Log gf
6021.118	$^{12}\text{C}^{14}\text{N}$	1.89	-1.750
6021.123	Gd I	0.84	-0.992
6021.129	$^{13}\text{C}^{14}\text{N}$	0.81	-2.098
6021.165	Ni I	5.28	-3.539
6021.275	Cr I	3.85	-2.593
6021.276	Ca I	5.58	-4.150
6021.299	$^{13}\text{C}^{14}\text{N}$	1.65	-1.600
6021.525	W I	2.24	-1.430
6021.526	$^{12}\text{C}^{14}\text{N}$	0.76	-2.982
6021.660	Sc I	2.11	-2.020
6021.710	$^{12}\text{C}^{14}\text{N}$	0.78	-2.216
6021.739	Sm II	1.38	-1.745
6021.746	Mn I	3.08	-2.822
6021.764	Ca I	5.59	-4.783
6021.772	Mn I	3.08	-1.605
6021.774	Mn I	3.08	-2.470
6021.787	Fe I	2.20	-4.253
6021.795	Mn I	3.08	-1.429
6021.798	Mn I	3.08	-2.345
6021.804	Mn I	3.08	-0.687
6021.813	Mn I	3.08	-1.403
6021.817	Mn I	3.08	-2.425
6021.820	Fe I	4.28	-4.109
6021.821	Mn I	3.08	-0.827
6021.827	Mn I	3.08	-1.470
6021.834	Mn I	3.08	-0.985
6021.837	Mn I	3.08	-1.646
6021.838	$^{13}\text{C}^{14}\text{N}$	0.74	-1.796
6021.843	Mn I	3.08	-1.169
6021.846	Mn I	3.08	-1.676

Table 2—Continued

$\lambda$ (Å)	Species	$\chi$ (eV)	Log gf
6021.847	Mn I	3.08	-1.391
6021.876	$^{12}\text{C}^{14}\text{N}$	0.84	-2.202
6021.880	$^{12}\text{C}^{14}\text{N}$	1.72	-1.907
6021.946	Cr I	3.85	-3.419
6022.102	Mo I	3.26	-1.473

Table 3. Non-LTE corrections

Star	$T_{\text{eff}}(\text{K})$	Log $g$	[Fe/H]	$\Delta_{\text{Non-LTE}}(6013\text{\AA})$	$\Delta_{\text{Non-LTE}}(6021\text{\AA})$
ROA213	4500	1.0	-2.0	+0.30	+0.32
ROA219	3900	0.7	-1.4	+0.12	+0.06
ROA236	4200	0.7	-1.2	+0.15	+0.09
ROA324	4000	0.7	-1.0	+0.11	+0.05
M4 2617	4280	1.2	-1.0	+0.11	+0.04

Note. —  $\Delta_{\text{Non-LTE}} = A_{\text{Non-LTE}} - A_{\text{LTE}}$ .

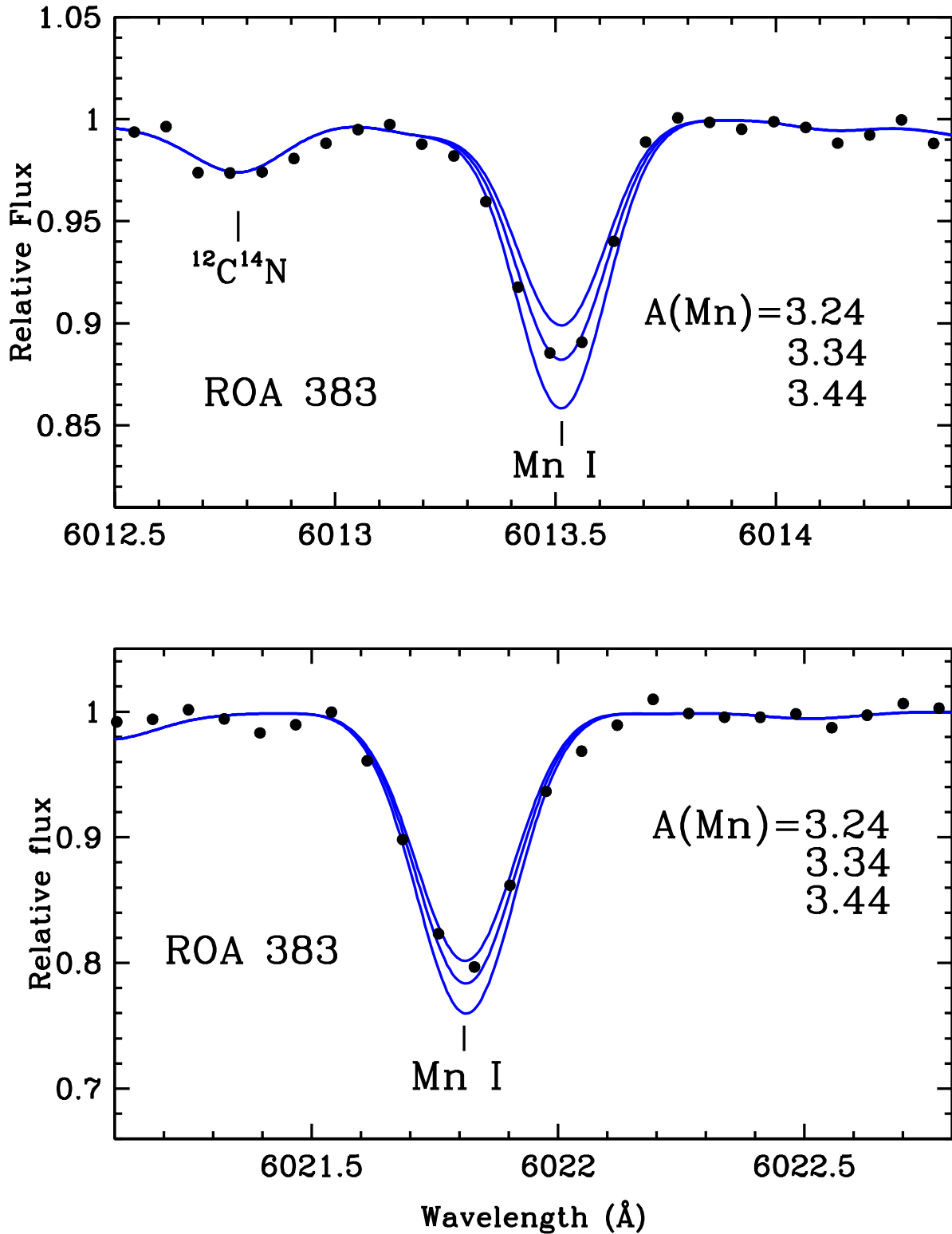


Fig. 1.— Sample observed spectra (dotted lines) in the region of the Mn I lines in target star ROA 383. Synthetic spectra (solid lines) were computed for 3 different Mn abundances ( $A(\text{Mn}) = 3.24; 3.34; 3.44$ ).

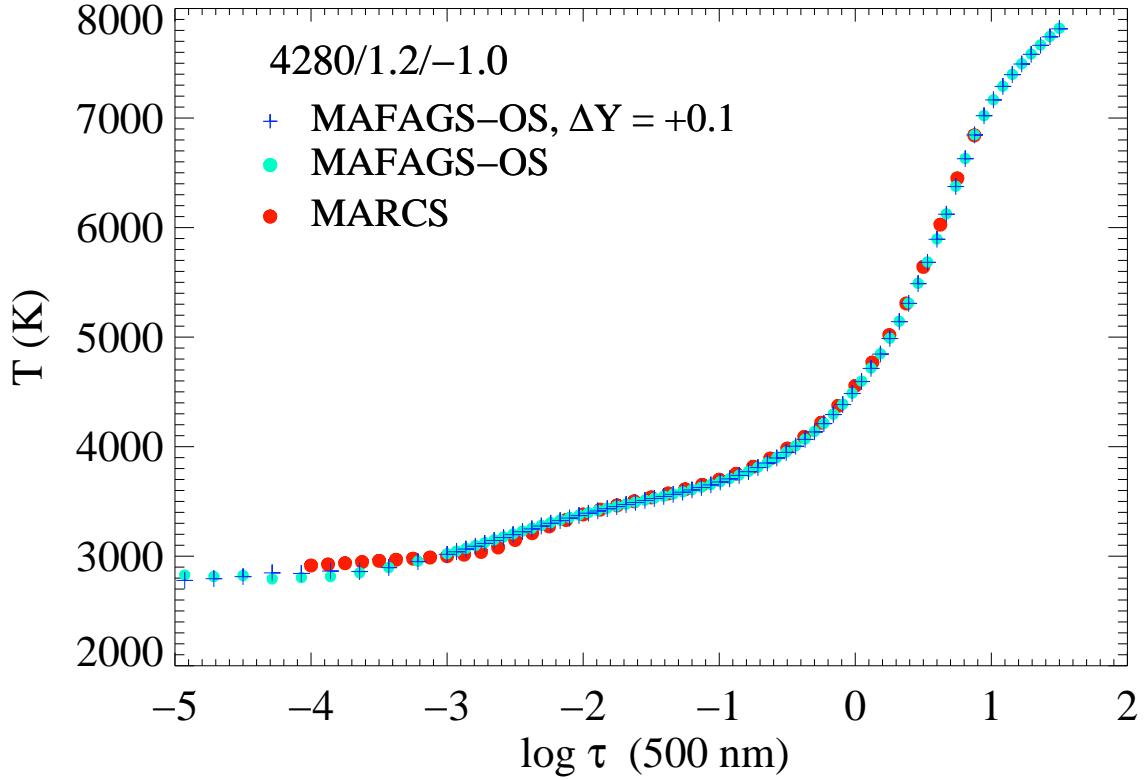


Fig. 2.— A comparison between the temperature stratification in the MAFAGS-OS model atmospheres (used to compute non-LTE corrections) with the model atmospheres adopted in the LTE analysis (Bell et al. 1976). We also show a model atmosphere computed with He mass fraction increased by 0.1 ( $\Delta Y = +0.1$ ) relative to the scaled-solar value ( $\Delta Y = 0$ ). The models correspond to  $T_{eff} = 4280$  K,  $\log g = 1.2$ ,  $[\text{Fe}/\text{H}] = -1.0$ .

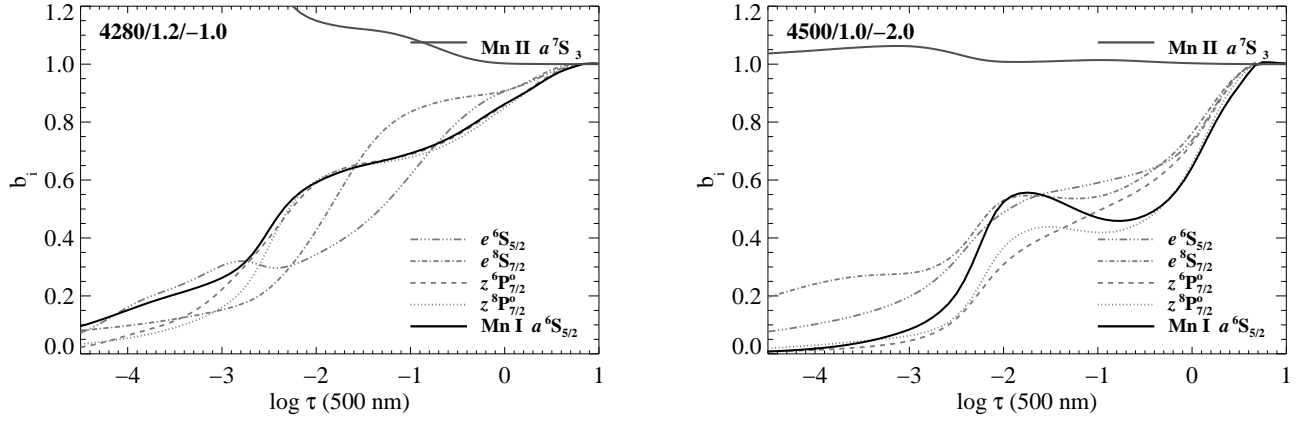


Fig. 3.— Departure coefficients  $b_i$  of selected Mn I levels as a function of continuum optical depth at 5000 Å. The model atmospheres are computed with stellar parameters specified in each panel.

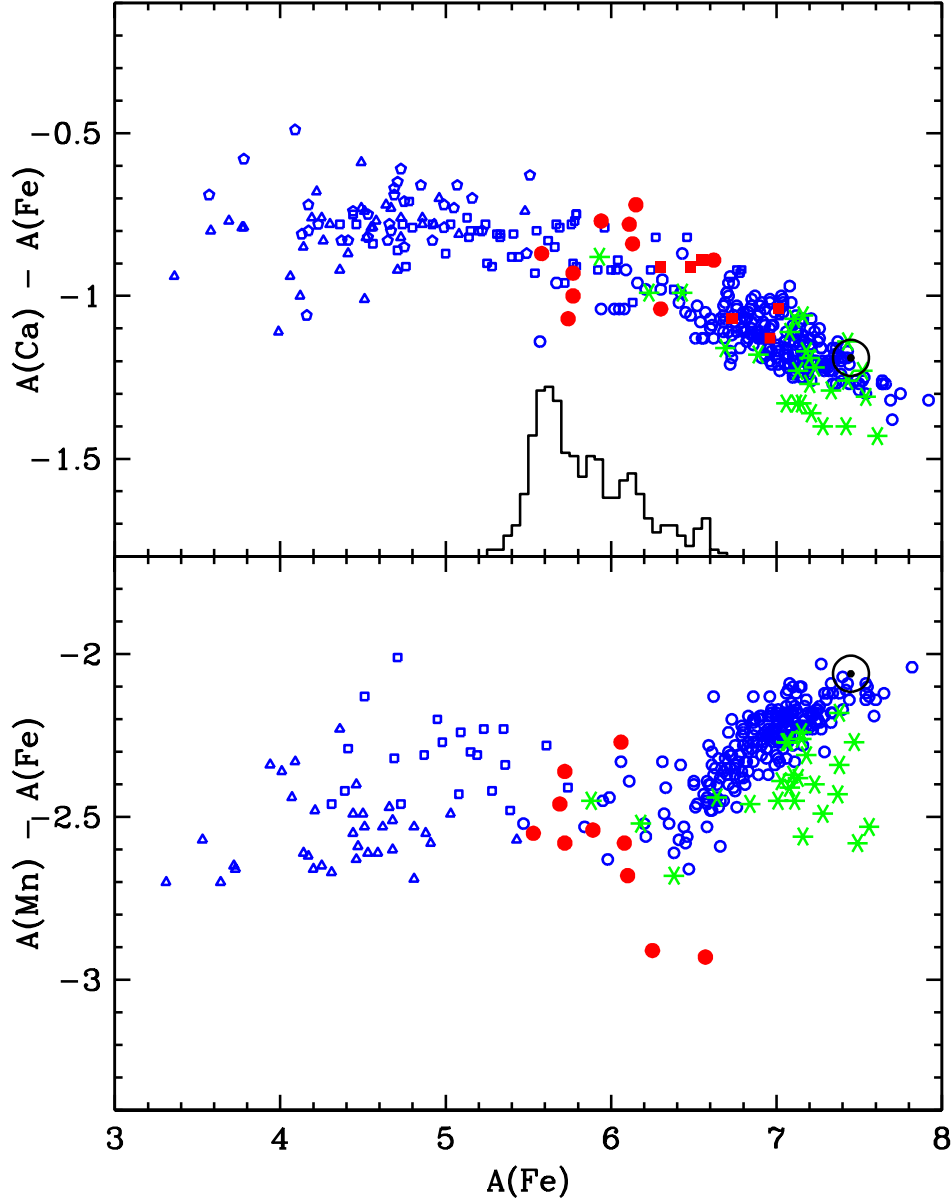


Fig. 4.— LTE calcium (top panel) and manganese (bottom panel) abundance results for  $\omega$  Cen in comparison with the Milky Way. The abundances for sample  $\omega$  Cen stars (red filled circles) are from this study and Smith et al. (2000). Calcium abundances for 6 additional targets in  $\omega$  Cen are from Pancino et al. (2002; red filled squares). The samples of stars representing the Milky Way disk and halo were taken from Reddy et al. (2003; 2006; blue open circles); Fulbright (2002; blue open squares); Johnson (2002; blue open squares); Cayrel et al. (2004; blue open triangles) and McWilliam et al. (1995; blue open pentagons). Abundance results for the Sagittarius dwarf galaxy by McWilliam et al. (2003) and Sbordone et al. (2007) are also shown (green asterisks). The metallicity distribution shown (top panel) is from Sollima et al. (2005).

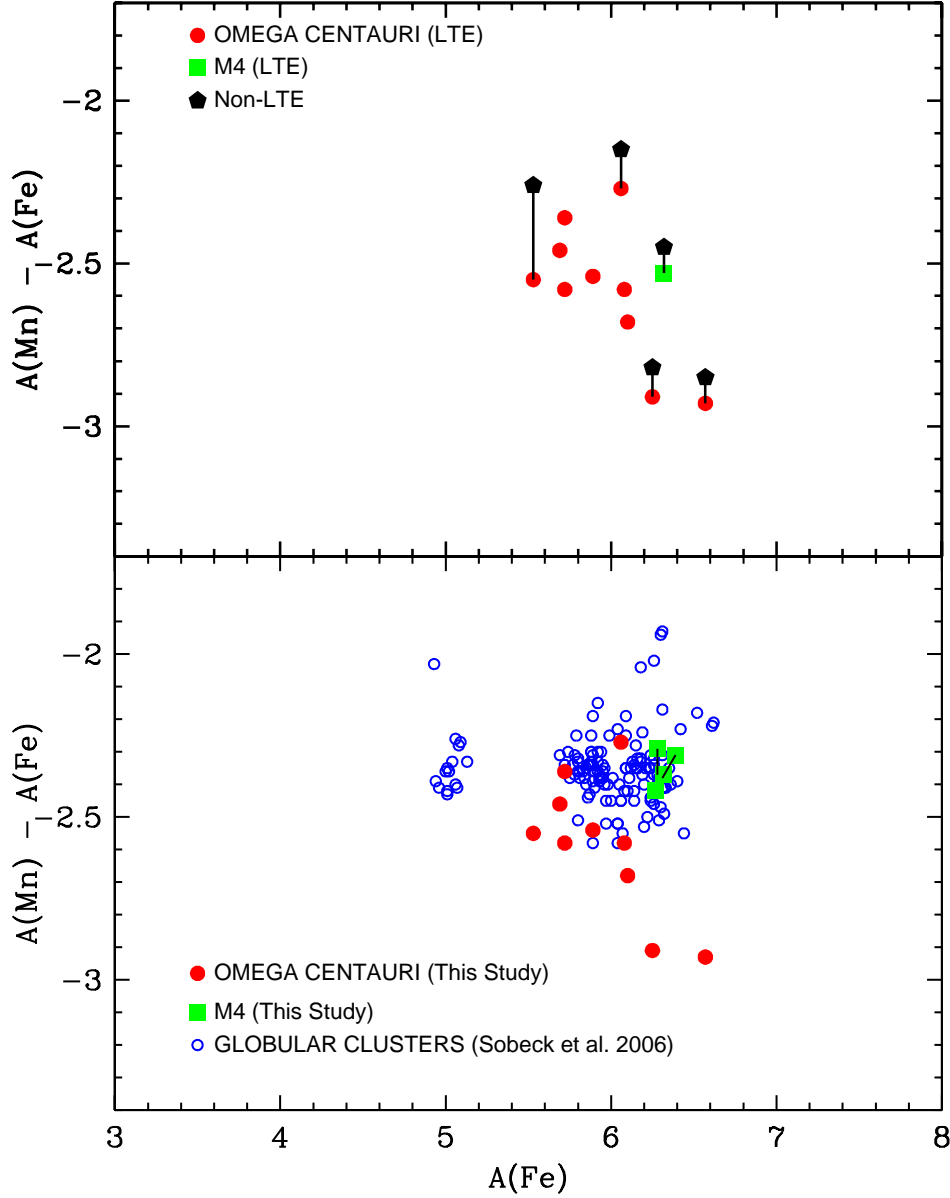


Fig. 5.— Top panel: LTE Mn results for  $\omega$  Cen (filled red circles) are shown along with the non-LTE corrections obtained for 5 targets. Note that the low  $[\text{Mn}/\text{Fe}]$  abundance of those stars representative of the more metal rich population in  $\omega$  Cen hold the same pattern in non-LTE. Bottom panel: The same LTE results for  $\omega$  Cen from top panel (red filled circles) shown in comparison with abundances derived for all globular clusters studied in Sobeck et al. (2006; blue open circles). M4 results are also shown (as filled green squares) and these emphasize the differences between Mn abundances in M4 and  $\omega$  Cen at a similar metallicity. Two M4 stars in this study are in common with the Sobeck et al. (2006) study and the derived Mn abundances are in good agreement within the uncertainties (connected by black solid lines). The Mn abundances in Sobeck et al. (2006) have been adjusted by 0.16 dex in order to be on the same log  $g_f$  scale as the results in this study.